# Frictional motion of normal-fluid component of superfluid $^3$He in aerogel

Ken Obara,* Chiaki Kato, Takaho Matsukura, Yusuke Nago, Ryusuke Kado, Hideo Yano, Osamu Ishikawa, and Toru Hata
*Department of Physics, Osaka City University, Sumiyoshi-ku, Osaka 558-8585, Japan*

Seiji Higashitani and Katsuhiko Nagai
*Graduate School of Integrated Arts and Sciences, Hiroshima University, Kagamiyama 1-7-1, Higashi-Hiroshima 739-8521, Japan*
(Received 2 June 2010; published 25 August 2010)

The superfluidity of liquid $^3$He in a high-porosity aerogel has been studied using a fourth-sound resonance technique. This technique has two significant advantages: it can directly determine the superfluid density and it can derive the transport properties of the viscous normal-fluid component. The temperature dependence of the resonance frequency revealed suppression of superfluidity and that a finite normal-fluid fraction exists even at $T=0$. The motion of the normal-fluid component has also been investigated. As $T\rightarrow 0$, the energy loss becomes very small, despite a finite amount of the normal-fluid component remaining. This implies that the normal-fluid component is highly constrained by the aerogel, and hence the dissipation mechanism cannot be described in terms of the conventional hydrodynamic model. We have succeeded to explain these results by introducing a frictional relaxation model to describe our observations, and found that the flow field changes from being parabolic (Hagen-Poiseuille viscous flow) to flat (Drude frictional flow) on introducing an aerogel. Numerical calculation of the relaxation time using the quasiclassical Green's-function method reproduces experimental results.

DOI: 10.1103/PhysRevB.82.054521 PACS number(s): 67.30.hm, 67.30.eh, 67.30.ht

## I. INTRODUCTION

Liquid $^3$He has attracted an academic interest because it is inherently highly pure and is a strongly correlated fermion system. Most of its basic properties have been extensively investigated and are consequently well understood.[1,2] Since, in the absence of a magnetic field, both the normal fluid and the superfluid B phase are completely isotropic, most properties can be understood in terms of the interaction represented by the Landau parameters, which depend only on pressure. Liquid $^3$He differs from electron systems such as those in conventional metals in that it has no charge nor lattice nor band structure. In this context, liquid $^3$He has been described as being a simple, ideal liquid. One of the most distinctive aspects of liquid $^3$He is its extremely long mean-free path. Even for normal liquid $^3$He the mean-free path of Landau quasiparticles varies as $1/T^2$ and is several micrometers at milikelvin temperatures. By cooling below the superfluid transition temperature $T_C$, the mean-free path of Bogoliubov quasiparticles, namely, the viscous transport mean-free path[3] $\lambda_\eta$ becomes extremely long. And by cooling far below $T_C$, $\lambda_\eta$ attains the size of the experimental cell. Introducing impurities into such a pure liquid in a well-controlled way is a very important way to investigate the basic transport phenomena of quasiparticles. Porous materials are useful to construct an impurity system in superfluid $^3$He. Among them, a silica aerogel is one of the materials whose porosity is the highest. The aerogel consists of interconnected and tangled chains of silica particles that are a few nanometers in diameter. The average distance between adjacent chains is on the order of a hundred nanometers. The porosity of the aerogel can be controlled chemically.[4] These characteristics provide an interesting system for investigating the superfluidity of liquid $^3$He since the average distance between adjacent chains $D$ is comparable to the superfluid coherence length $\xi_0$ and is much smaller than $\lambda_\eta$. In addition, the chain diameter $d$ is smaller than $\xi_0$ but larger than the Fermi wavelength $\lambda_F$,

$$\lambda_F < d < \xi_0 \sim D \ll \lambda_\eta. \tag{1}$$

This length scale indicates that the aerogel behaves as an impurity rather than a wall in superfluid $^3$He. Indeed, the suppression of the transition temperature $T_C$ and the superfluid density fraction $\rho_s/\rho$ have been found by various experimental methods.[5–10] These results demonstrate that the normal-fluid density remains finite at $T=0$ even in a high-porosity aerogel. However, the dynamic properties of the normal-fluid component are not yet determined. Our motivation is to understand the motion or the flow state of the residual normal-fluid component at very low temperatures.

## II. FOURTH SOUND

In this study, we employ the fourth-sound resonance technique. The fourth sound is a compression wave propagating through a *superleak*. The superleak is the structure that blocks the motion of the normal-fluid component due to its finite viscosity and allows only the superfluid component to pass through. For a straight cylindrical path of radius $R$, this condition is characterized by the inequality

$$\delta_v = \sqrt{\frac{2\eta}{\rho_n \omega}} \gg R, \tag{2}$$

where $\delta_v$ is the viscous penetration depth, $\eta$ is the shear viscosity, $\rho_n$ is the density of the normal component, and $\omega$ is the angular frequency of the fluid motion. The time evolution for the velocities of the normal fluid $\boldsymbol{v}_n$ and of the superfluid $\boldsymbol{v}_s$ are described by the following equations, which account for two-fluid hydrodynamics:

 

$$\rho_s \frac{\partial \boldsymbol{v}_s}{\partial t} = -\frac{\rho_s}{\rho} \nabla P + \rho_s S \nabla T, \tag{3}$$

$$\rho_n \frac{\partial \boldsymbol{v}_n}{\partial t} = -\frac{\rho_n}{\rho} \nabla P - \rho_s S \nabla T + \eta \nabla^2 \boldsymbol{v}_n, \tag{4}$$

and the mass and entropy conservation laws. Here, $\rho = \rho_s + \rho_n$ is the total density, $\rho_s$ is the density of the superfluid component, $P$ is the pressure, $T$ is the temperature, and $S$ is the entropy. In the case of an ideal superleak, the normal component is completely immobile, hence,

$$\rho_s/\rho = (c_4/c_1)^2, \tag{5}$$

where $c_1$ and $c_4$ represent the first- and fourth-sound velocities, respectively. The superfluid density can be obtained directly from Eq. (5). The first experiment using superfluid $^3$He was performed by Kojima *et al.*[11] In the case of an actual superleak, the clamping force is not strong enough, thus allowing the normal component to oscillate. The flow of the normal component $\rho_n \boldsymbol{v}_n$ is described by Hagen-Poiseuille flow, which has a parabolic flow profile. Jensen *et al.*[12] demonstrated that the dispersion relation for the fourth sound in a cylindrical channel for $R \ll \delta_v$ is given by

$$\omega^2 = c_4^2 q^2 - i\omega q^2 \frac{\rho_n}{\rho} c_1^2 \frac{1}{8} R^2 \frac{\rho_n}{\eta} \left[ 1 + \frac{4\zeta}{R} \right], \tag{6}$$

where $q$ represents the wave number and $\zeta$ is the slip length.[3] This dispersion relation reveals two important things. First, neither a finite viscosity nor a nonzero slip length contributes to the velocity of the fourth sound because the real part of Eq. (6) follows the linear dispersion relation $\omega = c_4 q$. No correction needs to be made irrespective of whether the dissipation is high or low. Second, the ratio of the imaginary part to the real part gives the energy loss,

$$Q^{-1} = \frac{\rho_n^2 R^2}{8 \eta \rho_s} \omega \left[ 1 + \frac{4\zeta}{R} \right] \tag{7}$$

$$= \frac{1}{4} \frac{\rho_n}{\rho_s} \left( \frac{R}{\delta_v} \right)^2 \left[ 1 + \frac{4\zeta}{R} \right]. \tag{8}$$

Equations (7) and (8) reveal that the energy loss is directly related to the motion of the normal component. This hydrodynamic theory in the viscous/slip regime was justified even for a complicated geometry like a sintered silver sponge superleak in a previous study by us.[13] Based on Eqs. (5) and (8), the fourth-sound resonance is considered to be an effective tool for studying the static and dynamic properties of a superfluid.

## III. EXPERIMENTAL

To study the motion of the normal-fluid component in an aerogel, we prepared an acoustic resonator with a 99.0% porosity aerogel, which is made of the same compound as the one used in an NMR experiment performed by our group.[14,15] We performed a small-angle neutron-scattering experiment using a large aerogel made from the same compound. The structural analysis revealed the existence of a weak spatial correlation with a characteristic length $l_a$ of approximately 128 nm. To prevent the aerogel chain from oscillating with the liquid, we grew the aerogel directly between particles of a sintered silver sponge. This sponge has a packing factor of 65%. The particles are almost spherical with a diameter of about 70 $\mu$m. We performed the fourth-sound experiment in pure $^3$He (i.e., with no aerogel) using an identical sintered silver sponge as the superleak. Although there was a discrepancy of approximately 10% between the bulk superfluid density fractions[16] measured using a torsional oscillator, the sintered silver sponge superleak exhibited no superfluid suppression due to the size effect and the effective pore radius was estimated to be $R = 10$ $\mu$m.[13] The resonator, which encases the sintered silver sponge in the aerogel, is cylindrical in shape with a diameter of 8.0 mm and a length $L$ of 15.0 mm. The schematic drawings of the cell are shown in Figs. 1(a) and 1(b).

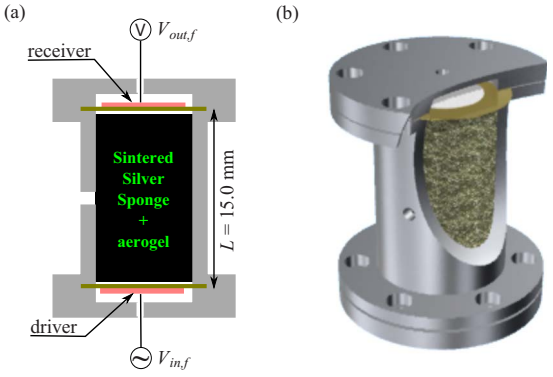


FIG. 1. (Color online) (a) Schematic drawings and (b) three-dimensional image of resonator. An inlet hole (1.0 mm in diameter) is located at the side face of the cylinder. The sintered silver sponge is well fixed to the wall of the cylinder. The driver and the receiver are made of the piezoelectric transducers. The space between the transducers and the sintered silver sponge is approximately 100 $\mu$m, and the amplitude of the transducer is less than 1 $\mu$m, so that the transducer never hits the sintered silver sponge. The length $L$ of the cavity corresponds to the distance between the driver and the receiver (see text for details).

The eigenfrequency of the aerogel chain for this setup is estimated to be more than 50 MHz,[17] which is a 100 times larger than the frequency band that is used in our experiment. Since the eigenoscillation of the aerogel chain is decoupled from the fluid oscillation during the resonance experiment, slow-mode oscillations[7] are not observed.

Measurements have been performed using a conventional frequency spectroscopy method. To drive and to detect the pressure oscillation, we used a piezoelectric transducers, as shown in Figs. 1(a) and 1(b). The transducers consist of a thin piezoceramics and a brass diaphragm, adapted to fit the cylinder size. In the spectroscopy method, an alternating voltage $V_{in,f} e^{i2\pi ft}$ is applied to the driver transducer to excite a pressure wave, and the voltage signal $V_{out,f} e^{i2\pi ft}$ is read from the receiver transducer, which is on the opposite side of the resonance cavity. If the resonance condition is satisfied, a large pressure oscillation is induced in the cell and a large $R(f) = V_{out,f}/V_{in,f}$ is obtained. The system is the dissipative

because the third term in Eq. (4) is finite. It means that there is a damping force proportional to the normal flow velocity. In this case, the frequency must be treated as a complex number, $f+i\gamma/2\pi$, where $f$ is the resonance frequency for the nondissipative case and $\gamma$ represents a damping factor. Under this condition, the measured spectra can be fitted by the following equation:

$$|R(f)|^2 = \sum_m \frac{R_m^2 f_m^4}{(f_m^2 - f^2)^2 + (\Delta f_m)^2 f^2}, \tag{9}$$

where $R_m$ is the $m$th mode amplitude, $f_m$ is the resonance frequency, and $\Delta f_m$ is the full width of the half maximum of the resonance. The acuity of $|R(f)|^2$ is measured as a quality factor $Q_m = f_m/\Delta f_m$. Since the analytical calculation gives that the linewidth is equal to the damping factor $\gamma$, $Q_m^{-1}$ expresses the dissipation per unit cycle. In this sense, we call $Q_m^{-1}$ the energy loss. A low $Q_m^{-1}$ means that the total damping force is low, which is observed as a very sharp spectrum.

The relationship between the energy loss and the attenuation is as follows. Suppose that a plane wave propagates along the $x$ axis without damping. It can be expressed as $\exp(ikx)$. In this case, the frequency is fixed but the wave number $k$ must be modified as

$$\omega = c_4(k + i\alpha), \tag{10}$$

and the propagating wave becomes $e^{-\alpha x}\exp(ikx)$, where $\alpha$ is the attenuation coefficient, the inverse of which is the characteristic attainable length of the wave. The fourth-sound velocity is derived from the real part of Eq. (10) and the damping factor is derived from the imaginary part. The ratio of the real to the imaginary part leads the energy loss. Finally, the relation between $Q_m^{-1}$ and $\alpha$ becomes

$$Q_m^{-1} = c_4\alpha/2\pi f_m. \tag{11}$$

In the case of fluid oscillation in a complicated geometry such as our sintered silver powder resonator, an acoustic refraction[18,19] must be taken into account as follows:

$$c_4 = 2n_a L f_m/m, \tag{12}$$

where $n_a = 1.402$ is the acoustic refraction index that is determined by the fourth-sound velocity measurements in superfluid $^4$He and is calibrated against the data table in Ref. 20. The superfluid fraction $\rho_s/\rho$ is calculated using Eq. (5), where $c_1$ is obtained from the table in Ref. 1, which has a negligibly small temperature dependence.

The measurements were performed in a zero magnetic field. The ambient pressure of the liquid $^3$He was adjusted to 2.89 MPa; at this pressure, the superfluid transition temperature $T_C^{(\mathrm{pure})}$ of pure $^3$He is 2.44 mK. The temperature was measured using a Pt NMR thermometer immersed in a bulk liquid; the thermometer was calibrated against a $^3$He melting curve thermometer.

## IV. RESULTS AND DISCUSSION

All the data given below were obtained during warming. A single measurement series was obtained by the following procedure. The sample was initially cooled to the minimum temperature (i.e., below 0.6 mK) and it was then gradually warmed in steps. The waiting time at each step was more than 1 h to allow the Pt NMR thermometer to stabilize. We performed this series several times and found good reproducibility. This measurement series could produce a uniform B-like phase, except at temperatures slightly below the superfluid transition temperature. The A-like phase might also exist but the quality factor of the resonance was too low (because of the preponderance of the normal-fluid component) to confirm this experimentally. On the other hand, during the cooling process we found an indication of an A-like to B-like phase transition and a state in which both phases coexist, as reported in Ref. 21. The A-like phase disappears at a temperature of $T_{A(-)} = 1.7$ mK. The phase transition in the aerogel is an interesting topic for study[9] but in this study we focus on the B-like region.

Figure 2 shows typical frequency spectra normalized by the excitation voltage. The excitation voltages, which are proportional to the maximum instantaneous pressure, were chosen so as to maximize the signal-to-noise ratio without inducing any nonlinear responses. We observed several resonance peaks corresponding to the $m$th harmonic resonance. Figure 2(b) shows an enlarged view of the spectrum $|R(f)|^2$, which is well fitted by Eq. (9) with a negligibly small error. The resonance frequencies decrease and the linewidths increase with increasing temperature, and the resonance disappears at a certain temperature $T_C$. The resonance frequencies depend very weakly on the temperature at low temperatures but they decrease abruptly near $T_C$. Since the frequency is related to the superfluid density [as shown in Eqs. (5) and (12)], the temperature dependence of the resonance frequency demonstrates that we have detected the fourth-sound resonance of superfluid $^3$He in an aerogel. Slow-mode resonance[7] was not observed; the reason for this is explained in Sec. III. The transition temperature at which the resonance disappears is $T_C = 2.27$ mK. The suppression factor was $T_C/T_C^{(\mathrm{pure})} = 0.938$. Figure 3(a) shows the temperature dependence of the sound velocity; it shows that there is no frequency dependence. The transition temperature $T_C$ obtained from the spectrum is identical to the intercept with the temperature axis for the fourth-sound velocity. Figure 4(a) shows the temperature dependence of the superfluid fraction $\rho_s/\rho$. Both the superfluid transition temperature and the superfluid density are suppressed. The pure superfluid resonator with a sintered silver sponge superleak has an identical structure to an aerogel resonator.[13] Since the sintered silver sponge superleak does not affect the superfluidity, the suppression of the superfluid transition temperature in the aerogel resonator is a result of the pair-breaking effect due to scattering between quasiparticles and the aerogel. We model this situation using the conventional homogeneous scattering model (HSM). In this model, the temperature dependence of the superfluid fraction in an impure system depends on the pair-breaking parameter $\tau T_C$ and the Landau parameter $F_1^s$. Here, $\tau T_C$ is a simple function of the suppression factor for the transition temperature $T_C/T_C^{(\mathrm{pure})}$, as shown in Fig. 5.[22] We found $\tau T_C = 5.8$ and the corresponding scattering time and mean-free path are $\tau = 19.4$ ns and $v_F\tau = 620$ nm, respectively. It is reasonable that the mean-free path of the quasiparticles is a few times longer than the correlation length $l_a$.

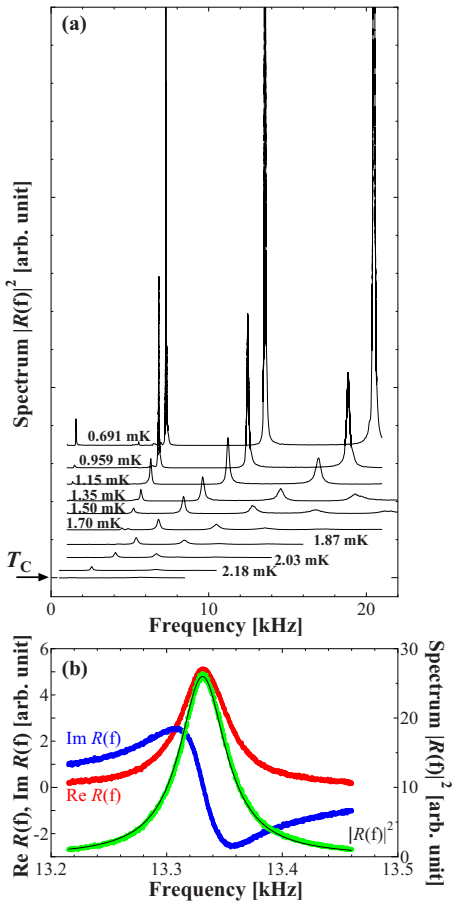


FIG. 2. (Color online) (a) Typical frequency spectra $|R(f)|^2$ at low temperatures. Each spectrum is normalized using the excitation voltage and vertically shifted according to its temperature. The peaks in the spectrum $T=0.691$ mK extend out of the display range; they indicate the sharpness of the spectrum. (b) Enlarged view of the spectrum at $T=0.783$ mK. The red, blue, and green symbols represent the in-phase oscillation amplitude Re $R(f)$, the out-of-phase oscillation amplitude Im $R(f)$, and the squared amplitude $|R(f)|^2$, respectively. The solid black line indicates Eq. (9) with fitting parameters $f_2=13332.188\pm0.023$ Hz and $\Delta f_2=49.003\pm0.065$ Hz. Thus, the energy loss is $Q_2^{-1}=(3.6755\pm0.0049)\times10^{-3}$.

Here, $v_F$ is the Fermi velocity of the $^3$He quasiparticles. Since there have been no theoretical or experimental studies on the Landau parameters of an impure Fermi liquid, we used the Landau parameter for pure $^3$He at 2.9 MPa (i.e., $F_1^s=13.3$).[23] The superfluid fraction was calculated using these parameters. The solid lines in Fig. 4(a) indicate the upper and lower limits for the superfluid density fraction. The red and blue lines indicate the Born and unitarity limits, respectively. Here, the Born limit corresponds to $N(0)v_{\rm imp}\ll1$ (weak scattering) and the unitarity limit to $N(0)v_{\rm imp}\to\infty$ (strong scattering), where $N(0)$ is the density of states at the Fermi level in the normal state and $v_{\rm imp}$ is the strength of the $s$-wave scattering potential. The calculation reproduces the experimental results well except at low temperatures. The corresponding density of states of the quasiparticles is shown in the Appendix.

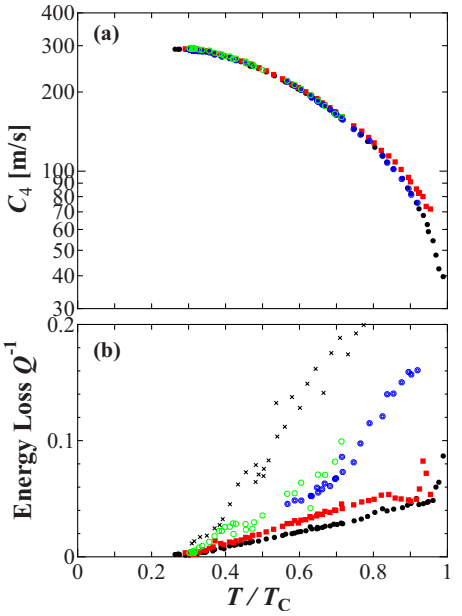


FIG. 3. (Color online) (a) Temperature dependence of fourth-sound velocity on warming. (b) Temperature dependence of energy loss of fourth sound. Black ●, red ■, blue ⓞ, and green ○ represent the second, third, fourth, and fifth harmonics, respectively. The × symbols represent $Q^{-1}$ of the second harmonic in a pure $^3$He fourth-sound resonator (Ref. 13).

We now discuss the energy loss of the fourth sound. Figure 3(b) shows the results for the energy loss of the fourth sound. We start from Eq. (8) to determine the temperature dependence of the energy loss. The × symbols show the results for a pure $^3$He fourth-sound resonator.[13] In the temperature range $0.3<T/T_C<0.8$, the energy loss decreases monotonically with decreasing temperature, reflecting the temperature dependence of the normal-fluid fraction. The shear viscosity is less important because its temperature dependence is weaker than that of the normal-fluid fraction, at least in this temperature range. ●, ■, ◎, and ○ symbols show the results obtained in this study for a resonator containing aerogel. We found that $Q_{\rm aero}^{-1}$ varies almost linearly with temperature. As shown in Fig. 4(b), $Q_{\rm aero}^{-1}$ is proportional to the frequency. These features are similar to the temperature dependence of $Q_{\rm pure}^{-1}$, which can be explained by hydrodynamic theory. We found that $Q_{\rm aero}^{-1}$ almost vanishes at a finite temperature of around $T/T_C=0.3$ despite there being a large amount of normal-fluid component in the aerogel at this temperature. Since the energy loss originates from normal-fluid motion, the normal-fluid component at low temperature must be highly constrained by the aerogel. Surprisingly, $Q_{\rm aero}^{-1}$ is approximately one fifth smaller than $Q_{\rm pure}^{-1}$. This implies that the magnitude of the drag force acting on the normal fluid in the aerogel is stronger than that in pure $^3$He. The shear viscosity $\eta$ cannot be responsible for this for the following reason. We consider the shear viscosity at $T_C$. In this case, the shear viscosity has its maximum value and it is possible to use transport theory for a normal-fluid state. According to the Landau-Boltzmann transport equation, the shear viscosity in the normal state of $^3$He that contains an impurity can be written as

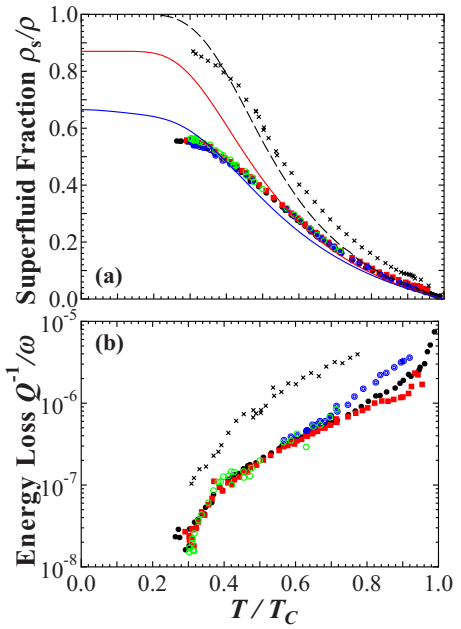


FIG. 4. (Color online) (a) Temperature dependence of superfluid fraction $\rho_s/\rho$. Black ●, red ■, blue ⓞ, and green ○ represent the second, third, fourth, and fifth harmonics, respectively. The dashed line shows the bulk superfluid density fraction at 29.2 bar (Ref. 16). The solid lines show the numerical calculation results for $\tau T_C=5.8$ and $F_1^s=13.3$ (see text for details). The red and blue lines correspond to the Born and unitarity limits, respectively. (b) Temperature dependence of energy loss of fourth-sound resonance divided by the resonance angular frequency. The four colors have the same meaning as for (a). The × symbols represent $Q^{-1}/\omega$ of the second harmonic in a pure $^3$He fourth-sound resonator (Ref. 13).

$$\eta = \frac{1}{5}\rho v_F^2(\tau_\eta^{-1} + \tau^{-1})^{-1}, \tag{13}$$

where $\tau_\eta = \lambda_\eta / v_F$ is the relaxation time that characterizes the viscosity. Here, $\lambda_\eta$ is the viscous mean-free path of the quasiparticles. The pure state is expressed by $\tau^{-1} \to 0$ but $\tau$ dominates when there is an aerogel since $\tau$ is on the order of the average aerogel chain length divided by $v_F$ and hence is much smaller than $\tau_\eta$. This means that the pure normal-state viscosity in the aerogel is strongly suppressed. There have not been any clear experimental results for the shear viscosity in a superfluid with an aerogel but it is plausible that the shear viscosity is also suppressed.[24] Since the energy loss $Q^{-1}$ is inversely proportional to the shear viscosity, the energy loss must be enhanced by the aerogel. This poses a problem: since the shear viscosity is reduced, the viscous penetration depth $\delta_v$ must also be reduced but we observed the fourth sound rather than the first sound. To prevent contradictions, we extend the damping mechanism to the hydrodynamic regime by rewriting the relaxation term in Eq. (4) as

$$\rho_n \frac{\partial \boldsymbol{v}_n}{\partial t} = -\frac{\rho_n}{\rho}\nabla P - \rho_s S \nabla T + \eta \nabla^2 \boldsymbol{v}_n - \boldsymbol{F}_d, \tag{14}$$

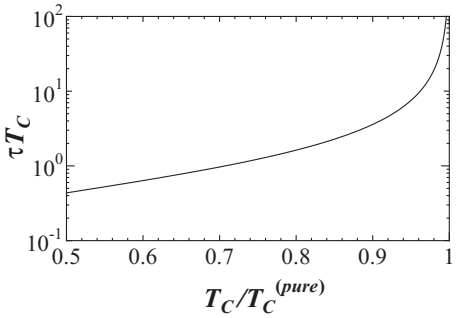


FIG. 5. Pair-breaking parameter $\tau T_C$ as a function of the suppression factor $T_C/T_C^{pure}$ in the HSM.

$$\delta_v = 1/|\mathrm{Im}\, k|, \quad k^2 = \frac{\rho_n}{\eta}(i\omega - \tau_f^{-1}), \tag{15}$$

where $\tau_f$ represents the relaxation time that characterizes the frictional drag force between the normal component and the aerogel. These two forces differ in that the viscous force depends on the spatial variation in $\boldsymbol{v}_n$, whereas the frictional force does not. The frictional drag force $\boldsymbol{F}_d$ is proportional to the normal-fluid velocity relative to the aerogel chain velocity $\boldsymbol{v}_a$; i.e.,

$$\boldsymbol{F}_d = \frac{\rho_n}{\tau_f}(\boldsymbol{v}_n - \boldsymbol{v}_a). \tag{16}$$

The frictional damping mechanism treats scattering between quasiparticles phenomenologically. The drag force to the normal fluid is generated by the momentum transfer from the quasiparticles to the aerogel chains.[17,25] This mechanism describes well the ultrasonic attenuation measurement in normal fluid performed by Nomura *et al.*[26] According to Eqs. (15) and (16), the viscous penetration depth is also modified as

$$\delta_v = \begin{cases} \sqrt{\dfrac{2\eta}{\rho_n \omega}} = \delta_{v,0} & (\text{for } \omega\tau_f \gg 1), \\ \sqrt{\dfrac{\eta\tau_f}{\rho_n}} = \delta_{v,a} & (\text{for } \omega\tau_f \ll 1). \end{cases} \tag{17}$$

The first case is the conventional type. However, in the second case, $\delta_{v,a}$ becomes extremely small because $\delta_{v,a}/\delta_{v,0} = \omega\tau_f/2$. This means that introducing the aerogel changes the flow profile from parabolic to flat. The flat velocity profile means that the normal-fluid component oscillates uniformly and simultaneously. This flow type is known as Drude flow[24] since it is analogous to the motion of the conduction electrons in conventional metals. In other words, we have experimentally found a new class of transition in which introducing an aerogel causes the normal-fluid component in the superfluid to lose its viscous nature and become frictional.

To gain a better understanding of the frictional force, we describe the frictional relaxation time $\tau_f$ in a little more detail. According to viscoelastic theory,[17] the dispersion relation becomes

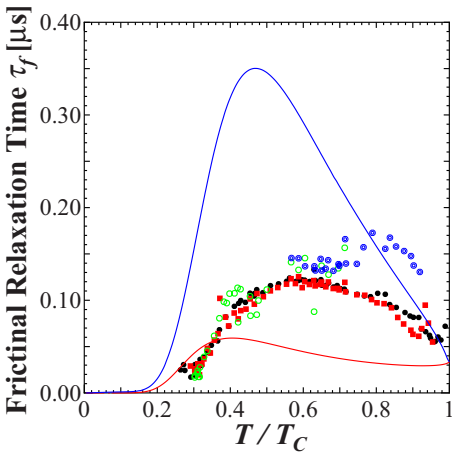


FIG. 6. (Color online) Temperature and mode dependence of frictional relaxation time $\tau_f(T)$. Black ●, red ■, blue ⓞ, and green ○ represent the second, third, fourth, and fifth harmonics, respectively. The solid line shows the numerical calculation results for $\tau T_C=5.8$ (see text for details). The red and blue lines correspond to the Born and unitarity limits, respectively.

$$(z^2-c_1^2)(z^2-c_2^2)+\left(i\frac{4\eta\omega}{3\rho_n}+\frac{iz^2}{\omega\tau_f}\right)(z^2-c_4^2)=0, \quad (18)$$

where $z$ is a complex velocity. On introducing Eq. (18), $\boldsymbol{v}_a\rightarrow 0$ is used because our experimental setup satisfies it as shown in Sec. III.

The sound velocity and the energy loss can be obtained as follows:

$$\mathrm{Re}\, z^2=c_4^2, \quad Q^{-1}=\frac{\rho_n}{\rho_s}\omega\tau_f+\mathcal{O}[(\omega\tau_f)^2]. \quad (19)$$

The first equation reveals why we observed the fourth-sound resonances despite the short viscous penetration depth: the oscillation of the normal component can be suppressed by a frictional force as efficiently as by a viscous force. The second equation shows that the energy loss is proportional to the frequency, which can be seen in Fig. 4(b). The fourth-sound velocity and the energy loss do not involve the shear viscosity term, which contributes only to the higher order term of $\omega\tau_f$. Figure 6 shows the frictional relaxation time calculated by Eq. (19). Almost all points appear on the same curve.[27] It shows the characteristic broad peak at $T_{\mathrm{peak}}\sim 0.6T_C$, which is quantitatively consistent with a numerical study that used a quasiclassical Green's-function technique with the HSM in a relatively clean system with $\tau T_C\gtrsim 1$.[28] We measured a small but finite-energy loss relative to pure $^3$He indicating that $\boldsymbol{v}_n-\boldsymbol{v}_a$ is small but finite. Since $\rho_n$ also remains finite, the drag force $\boldsymbol{F}_d$ is simply inversely proportional to $\tau_f$, as shown in Eq. (16). This is consistent with $\tau_f$ decreasing to almost zero at a finite temperature. We give new numerical calculation results below. According to the theory, generally two adjustable parameters are needed to characterize the system: $\tau T_C$, which is already determined by the suppression of $T_C$ and $\tau_f$ at the transition temperature $T_C$. We obtained $\tau_f(T_C)$ in the following manner. According to the Landau transport theory, $\tau_f(T_C)$ and the scattering rate $\tau^{-1}$ are related by $\tau_f(T_C)=(m/m^*)\tau$, where $\tau=19.4$ ns has already been obtained and $m^*/m=5.8$ is the effective-mass ratio of the quasiparticles.[23] We found $\tau_f(T_C)=0.334$ $\mu$s. The theory predicts that all the experimental data should lie between the curves of the Born and unitarity limits. The solid lines in Fig. 6 show the results for the numerical calculation within the HSM. Although there are little differences, and despite using the parameter for the pure $^3$He, the numerically obtained relaxation time qualitatively reproduces the experimental observations, i.e., the peak structure, the order of the relaxation time, and the relaxation time at $T_C$. Hence, we have demonstrated the effectiveness of our frictional relaxation model; the drag force acting on the normal-fluid component at the lowest temperature is not the viscous force but the frictional force that originates from the momentum transfer from the quasiparticle to the aerogel during scattering. The microscopic spatial distribution of the normal-fluid component is an interesting subject but it lies beyond the scope of the present theory. For this, a more elaborate theory is required that accounts for the aerogel structure in detail.

## V. SUMMARY

We studied the motion of the normal-fluid component in superfluid $^3$He immersed in a high-porosity aerogel by a fourth-sound resonance technique. From the resonance frequency, we found that both the transition temperature and the superfluid fraction are suppressed. From the suppression of superfluid transition temperature, we theoretically calculated the superfluid fraction using the HSM, which reproduced the experimental results well. From the shape of the resonance spectra, we obtained the energy loss of the fourth sound due to motion of the normal-fluid component. We found that the energy loss in a resonator that contains an aerogel is smaller than that in a pure superfluid resonator, and it decreases to almost zero at a finite temperature despite retaining a finite amount of the normal component. This means that the residual normal-fluid component is highly constrained by the aerogel. We showed that the dissipation mechanism had changed from a conventional viscous mechanism to a frictional mechanism. Introducing the aerogel changed the flow field changed from parabolic (Hagen-Poiseuille) to flat (Drude). The temperature dependence of the relaxation time that characterizes the friction between the normal-fluid component and the aerogel was obtained experimentally. The numerically obtained relaxation time qualitatively reproduced the experimental observations.

## ACKNOWLEDGMENTS

We would like to thank Aizawa and Morii of the Neutron Science Research Center of Japan Atomic Energy Research Institute who analyzed the neutron-scattering structure of our aerogel. We would also like to thank Yokogawa and Yokoyama of Matsushita Electric Works for donating the aerogel samples. This work was supported by a Grant-in-Aid for Scientific Research from the Ministry of Education, Science and Culture, Japan (Grant No. 17071009).

## APPENDIX: DENSITY OF STATES OF QUASIPARTICLES

In Sec. IV, we calculated the superfluid density fraction using the homogeneous scattering model with $\tau T_C = 5.8$. It is also possible to calculate the density of states of the quasiparticles in aerogel, $n(\epsilon)$. Figure 7 shows the density of states for several temperatures as a function of the energy difference from the Fermi level $\epsilon$ normalized by the off-diagonal part of the superfluid Hamiltonian at $T=0$, $\Delta_{BW}(0)$. In the Born limit, a simple gap around the Fermi level appears at all temperatures. However, in the unitarity limit, new quasiparticle states emerge between the energy gap at all temperatures. At higher temperatures, the structure of the density of states strongly depends on the temperature; however, it exhibits very little temperature dependence below $T/T_C = 0.6$. The existence of a finite density of states at the Fermi level is consistent with the findings of Choi *et al.*[10] and Sharma and Sauls.[29] However, in our high-porosity aerogel, the impurity band is located well below the gap edge and the gap width is approximately half of $k_B T_C$, whereas that for a 98% aerogel extends up to the gap edge or even completely fills the gap. This is a significant point for a high-porosity aerogel.

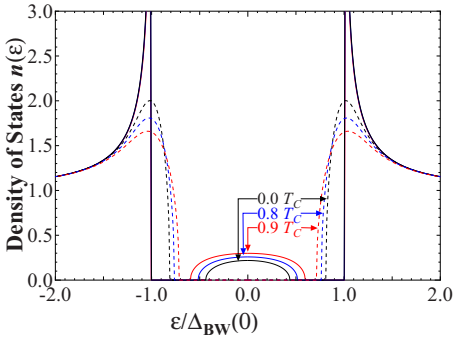


FIG. 7. (Color online) Temperature dependence of density of states as a function of the energy difference from the Fermi level normalized by the BCS gap at $T=0$ for pair-breaking parameter $\tau T_C = 5.8$. The solid and dashed lines represent the unitarity and Born limits, respectively.

*obara@sci.osaka-cu.ac.jp


[1] J. C. Wheatley, Rev. Mod. Phys. **47**, 415 (1975).
[2] A. J. Leggett, Rev. Mod. Phys. **47**, 331 (1975).
[3] D. Einzel and J. Parpia, J. Low Temp. Phys. **109**, 1 (1997).
[4] A. S. Dorcheh and M. H. Abbasi, J. Mater. Process. Technol. **199**, 10 (2008).
[5] D. T. Sprague, T. M. Haard, J. B. Kycia, M. R. Rand, Y. Lee, P. J. Hamot, and W. P. Halperin, Phys. Rev. Lett. **75**, 661 (1995).
[6] J. V. Porto and J. M. Parpia, Phys. Rev. B **59**, 14583 (1999).
[7] A. Golov, D. A. Geller, J. M. Parpia, and N. Mulders, Phys. Rev. Lett. **82**, 3492 (1999).
[8] P. Brussaard, S. N. Fisher, A. M. Guenault, A. J. Hale, N. Mulders, and G. R. Pickett, Phys. Rev. Lett. **86**, 4580 (2001).
[9] J. E. Baumgardner and D. D. Osheroff, Phys. Rev. Lett. **93**, 155301 (2004).
[10] H. Choi, K. Yawata, T. M. Haard, J. P. Davis, G. Gervais, N. Mulders, P. Sharma, J. A. Sauls, and W. P. Halperin, Phys. Rev. Lett. **93**, 145301 (2004).
[11] H. Kojima, D. N. Paulson, and J. C. Wheatley, Phys. Rev. Lett. **32**, 141 (1974).
[12] H. Jensen, H. Smith, and P. Wölfle, J. Low Temp. Phys. **51**, 81 (1983).
[13] Y. Nago, C. Kato, K. Obara, H. Yano, O. Ishikawa, and T. Hata, J. Low Temp. Phys. **150**, 476 (2008).
[14] R. Kado, H. Nakagawa, K. Obara, H. Yano, O. Ishikawa, and T. Hata, J. Low Temp. Phys. **148**, 585 (2007).
[15] H. Nakagawa, R. Kado, K. Obara, H. Yano, O. Ishikawa, T. Hata, H. Yokogawa, and M. Yokoyama, Phys. Rev. B **76**, 172504 (2007).
[16] J. M. Parpia, D. G. Wildes, J. Saunders, E. K. Zeise, J. D. Reppy, and R. C. Richardson, J. Low Temp. Phys. **61**, 337 (1985).
[17] M. Miura, S. Higashitani, M. Yamamoto, and K. Nagai, J. Low Temp. Phys. **134**, 843 (2004).
[18] D. L. Johnson, Appl. Phys. Lett. **37**, 1065 (1980).
[19] D. L. Johnson and P. N. Sen, Phys. Rev. B **24**, 2486 (1981).
[20] J. Maynard, Phys. Rev. B **14**, 3868 (1976).
[21] Y. Nago, K. Obara, R. Kado, H. Yano, O. Ishikawa, and T. Hata, J. Low Temp. Phys. **148**, 597 (2007).
[22] $k_B = \hbar = 1$ was used in this theory. This corresponds to $\tau k_B T_C/\hbar$ in the MKSA system of units.
[23] E. R. Dobbs, *Helium Three* (Oxford University Press, New York, 2000), Chap. 3, p. 51.
[24] D. Einzel and J. M. Parpia, Phys. Rev. Lett. **81**, 3896 (1998).
[25] T. Ichikawa, M. Yamamoto, S. Higashitani, and K. Nagai, J. Phys. Soc. Jpn. **70**, 3483 (2001).
[26] R. Nomura, G. Gervais, T. M. Haard, Y. Lee, N. Mulders, and W. P. Halperin, Phys. Rev. Lett. **85**, 4325 (2000).
[27] Except the fourth mode whose frequency spectrum $R(f)$ is asymmetric.
[28] S. Higashitani, M. Miura, M. Yamamoto, and K. Nagai, Phys. Rev. B **71**, 134508 (2005).
[29] P. Sharma and J. Sauls, J. Low Temp. Phys. **125**, 115 (2001).